Inorg. Chem. **2007**, *46*, 8752–8762

Inorganic Chemistry
Article

Spectroscopic and Computational Studies of a Ru(II) Terpyridine Complex: The Importance of Weak Intermolecular Forces to Photophysical Properties

Claudio Garino,[†] Roberto Gobetto,*,[†] Carlo Nervi,[†] Luca Salassa,[†,‡] Edward Rosenberg,*,[‡] J. B. Alexander Ross,[‡] Xi Chu,[‡] Kenneth I. Hardcastle,[§] and Cristiana Sabatini[||]

Dipartimento di Chimica IFM, Università di Torino, Via P. Giuria 7, I-10125 Torino, Italy, Department of Chemistry, University of Montana, Missoula, Montana 59812, Department of Chemistry, Emory University, 1515 Dickey Drive, Atlanta, Georgia 30322, and Istituto per la Sintesi Organica e la Fotoreattività del CNR, Via P. Gobetti 101, I-40129 Bologna, Italy

Received May 28, 2007

The complex $[Ru(tpy)(CO)_2TFA]^+[PF_6]^-$ (where tpy = 2,2′:6′,2″-terpyridine and TFA = $CF_3CO_2^-$) (**1**) has been synthesized and fully characterized spectroscopically. The X-ray structure of the complex has been determined. The photopysical properties of the ruthenium complex and the free ligand tpy have been investigated at room temperature and at 77 K in acetonitrile solution and in the solid state. Their electronic spectra are highly influenced by intermolecular stacking interactions, both in solution and in the solid state. Density functional theory (DFT) and time-dependent DFT (TDDFT) calculations have been performed to characterize the electronic structure and the excited states of $[Ru(tpy)(CO)_2TFA]^+[PF_6]^-$ and tpy. TDDFT calculations on three different conformations of free ligand have been performed as well. Absorption and emission spectra of tpy have been studied at different temperatures and concentrations in order to have a better understanding of this ruthenium derivative's properties. The absorption spectrum of **1** is characterized by metal-perturbed ligand-centered (LC) bands in the UV region. No metal-to-ligand charge transfer (MLCT) bands are observed in the visible for the complex. Only at high concentrations (10^{-4} M) does a very weak band appear at 470 nm. At 77 K and low concentrations, solutions of **1** exhibit a major ^{3}LC emission band centered at 468 nm (21.4×10^{-3} cm^{-1}). When the concentration of the complex is increased, an unstructured narrow emission at 603 nm (16.6×10^{-3} cm^{-1}), with a lifetime of 10 μs, dominates the emission spectrum in glassy acetonitrile. This emission originates from a π–π stacked dimeric (or oligomeric) species. TDDFT calculations performed on a tail-to-tail dimer structure, similar to that seen in the solid state, ascribe the transition to a triplet excited state, where intermolecular metal (d) → ligand (π^*, polypyridine) charge transfer occurs. A good estimate of the transition energy is also obtained (623 nm, 1.94 eV).

Introduction

Supramolecular chemistry is one of the most active fields in coordination chemistry for applications in new nanomaterials and biological systems. Noncovalent intermolecular interactions,[1] such as hydrogen bonds or $\pi-\pi$ stacking,[2] are crucial for both DNA and proteins.[3] They govern molecular association, catalysis, and a multitude of biochemical processes.[4−7] Noncovalent interactions can drive chemical reactions by promoting the formation of stable

---

* To whom correspondence should be addressed. E-mail: roberto.gobetto@unito.it (R.G.).

[†] Università di Torino.

[‡] University of Montana.

[§] Emory University.

[||] Istituto per la Sintesi Organica e la Fotoreattività del CNR.

(1) Desiraju, G. R. *Acc. Chem. Res.* **2002**, *35*, 565−573.

(2) Hunter, C. A.; Sanders, J. K. M. *J. Am. Chem. Soc.* **1990**, *112*, 5525−5534.

(3) Moran, L. A.; Scrimgeour, K. G.; Horton, H. R.; Ochs, R. S.; Rawn, J. D. *Biochemistry*; Neil Patterson Publishers/Prentice Hall: Englewood Cliffs, NJ, 1994.

(4) Jeffrey, G. A.; Saenger, W. *Hydrogen Bonding in Biological Structures*; Springer-Verlag: Berlin, 1991.

(5) Zhang, X. X.; Bradshaw, J. S.; Izatt, R. M. *Chem. Rev.* **1997**, *97*, 3313−3362.

(6) Ojima, I. *Catalytic Asymmetric Synthesis*; Wiley-VCH: Chichester, U.K., 2000.

(7) Zanoni, G.; Castronovo, F.; Franzini, M.; Vidari, G.; Giannini, E. *Chem. Soc. Rev.* **2003**, *32*, 115−129.

10.1021/ic7010343 CCC: $37.00

three-dimensional aggregates and thus shifting the reaction equilibria.[8−10]

Supramolecular systems, which involve weak noncovalent interactions, exhibit environmentally sensitive spectroscopic properties (e.g., polar solvents, temperature, pH).[11] Nevertheless, the study of these systems is an open challenge for potential applications in highly responsive materials and for the development of noncovalently coupled large systems. The energy transfer process between covalently bound dimeric metal complexes has been widely investigated,[12] but very few examples of noncovalent dimers have been studied. Among these systems there are hydrogen-bonded supramolecular aggregates containing octahedral ruthenium and osmium diimine units[13,14] and square planar platinum diimine units.[15−17]

2,2′:6′,2″-Terpyridine[18] (tpy) platinum complexes have been shown to form $\pi-\pi$ stacked dimers or oligomers. Complexes of general formula [Pt(tpy)L] (where L = Cl, Me, Ph, NCS, OH, OMe) give supramolecular architectures in solution due to ($\pi-\pi$) ligand−ligand interactions and metal−metal interactions.[15−17] These interactions noticeably influence the electronic spectrum of the complexes, e.g., low-energy $d\sigma^* \rightarrow \pi^*$(polypyridine) excited states.

This behavior, to the best of our knowledge, has never been reported for octahedral ruthenium complexes containing a tpy ligand, in spite of several studies on ruthenium-terpyridine derivatives forming $\pi-\pi$ stacked aggregates.[19]

In this paper, we report a study on the complex $[Ru(tpy)(CO)_2TFA]^+[PF_6]^-$ (where TFA = $CF_3CO_2^-$) and its concentration-dependent photophysical properties due to $\pi-\pi$ stacking and weak intermolecular hydrogen bonds. Our focus on this complex rather than the known $[Ru(tpy)(CO)_2Cl]^+[PF_6]^-$ [20,21] has been motivated by the fact that the TFA ligand increases the intermolecular interactions by means of its polar groups, and thus facilitates the formation of supramolecular aggregates.

Terpyridine ruthenium complexes usually display weak or no emissions at room temperature,[22] because the value of the bite angle of tpy is not ideally suited for octahedral coordination. This causes a weak ligand field at the metal and thus a low energy of the triplet metal-centered (^{3}MC) state, which provides a faster efficient nonradiative thermally activated decay pathways.[12,23,24] As a result, tpy metal complexes are usually weak emitters with very short lifetimes (from 250 ps to 40 ns).

In the case of $[Ru(tpy)(CO)_2TFA]^+[PF_6]^-$, no metal-to-ligand-charge-transfer (MLCT) bands are visible in the absorption spectrum. Emission properties of the complex can be related to the metal-perturbated tpy with little contribution from the ruthenium atom. However, the formation of supramolecular species was observed performing experiments at variable concentration and at different temperatures. An assignment of the emission properties of these species is proposed in this work, together with a computational study of the excited-state properties.

We also report a study on the photophysical properties of free tpy for a better understanding of the complex behavior.

Experimental Section

Materials and Methods. All reagents were purchased from Aldrich and used as received. All solvents were reagent grade and purified by standard techniques where required.[25]

Ruthenium carbonyl was purchased from STREM Chemicals, and microanalyses were performed by Schwarzkopf Analytical Laboratories, Woodside, New York.

NMR spectra were recorded on a JEOL EX 400 spectrometer (B_0 = 9.4 T, ^{1}H operating frequency 399.78 MHz) with chemical shifts referenced to residual protons in the solvent (acetone-d_6 or methanol-d_4). IR spectra were recorded as powder-ATR using a Thermo-Nicolet 670 FT-IR spectrophotometer with 1 cm^{-1}-resolution and 64 scans.

UV−vis absorption spectra were measured with a DR LANGE CADAS 200 spectrophotometer; room-temperature and low-temperature emission spectra, as well as luminescence lifetimes were obtained using a HORIBA Jobin Yvon IBH Fluorolog-TCSPC spectrofluorimeter.

Luminescence lifetimes were determined by time-correlated single-photon counting using excitation with nanosecond pulses of 297 or 455 nm light at repetition rates ranging from 1 MHz to 10 kHz generated by a NanoLed pulsed diode. The emission data were collected using a spectral bandwidth of 10 nm. The data were collected into 2048 channels to 10000 counts in the peak channel.

The sample was maintained at 20 °C in an automated sample chamber (F-3004 Peltier Sample Cooler from Horiba Jobin Yvon IBH) for ambient temperature measurements while low-temperature measurements were carried out by immersion of the sample held in a quartz tube in liquid N_2.

The emission decay data were analyzed using the software DAS6 (TCSPC Decay Analysis Software), provided with the instrument. Decays longer than 1 μs were fit directly without reconvolution as sums of exponentials because the excitation pulse is essentially a delta function at this time resolution. Decays shorter than 1 μs were

---

(8) Oh, K.; Jeong, K. S.; Moore, J. S. *Nature* **2001**, *414*, 889−893.
(9) Kirshenbaum, K.; Zuckermann, R. N.; Dill, K. A. *Curr. Opin. Struct. Biol.* **1999**, *9*, 530−535.
(10) Stigers, K. D.; Soth, M. J.; Nowick, J. S. *Curr. Opin. Chem. Biol.* **1999**, *3*, 714−723.
(11) Huber, R. *Angew. Chem., Int. Ed.* **1989**, *28*, 848−869.
(12) Balzani, V.; Juris, A.; Venturi, M.; Campagna, S.; Serroni, S. *Chem. Rev.* **1996**, *96*, 759−833.
(13) Ward, M. D.; Barigelletti, F. *Coord. Chem. Rev.* **2001**, *216*, 127−154.
(14) Rau, S.; Schafer, B.; Schebesta, S.; Grussing, A.; Poppitz, W.; Walther, D.; Duati, M.; Browne, W. R.; Vos, J. G. *Eur. J. Inorg. Chem.* **2003**, 1503−1506.
(15) Bailey, J. A.; Hill, M. G.; Marsh, R. E.; Miskowski, V. M.; Schaefer, W. P.; Gray, H. B. *Inorg. Chem.* **1995**, *34*, 4591−4599.
(16) Aldridge, T. K.; Stacy, E. M.; McMillin, D. R. *Inorg. Chem.* **1994**, *33*, 722−727.
(17) Arena, G.; Calogero, G.; Campagna, S.; MonsùScolaro, L.; Ricevuto, V.; Romeo, R. *Inorg. Chem.* **1998**, *37*, 2763−2769.
(18) Constable, E. C. *Chem. Soc. Rev.* **2007**, *36*, 246−253.
(19) Franco, M.; Araki, K.; Rocha, R. C.; Toma, H. E. *J. Solution Chem.* **2000**, *29*, 667−684.
(20) Gibson, D. H.; Sleadd, B. A.; Mashuta, M. S.; Richardson, J. F. *Organometallics* **1997**, *16*, 4421−4427.
(21) Gibson, D. H.; Andino, J. G.; Bhamidi, S.; Sleadd, B. A.; Mashuta, M. S. *Organometallics* **2001**, *20*, 4956−4964.
(22) Hofmeier, H.; Schubert, U. S. *Chem. Soc. Rev.* **2004**, *33*, 373−399.
(23) Calvert, J. M.; Caspar, J. V.; Binstead, R. A.; Westmoreland, T. D.; Meyer, T. J. *J. Am. Chem. Soc.* **1982**, *104*, 6620−6627.
(24) Sauvage, J. P.; Collin, J. P.; Chambron, J. C.; Guillerez, S.; Coudret, C.; Balzani, V.; Barigelletti, F.; Decola, L.; Flamigni, L. *Chem. Rev.* **1994**, *94*, 993−1019.
(25) Amarengo, W. L. F.; Perrin, D. D. *Purification of Laboratory Chemicals*; Butterworth-Heinemann: Oxford, 1998.

fit with reconvolution of the time-dependent profile of the light source. The best fit was assessed on the basis of the parameter χ^2, which was close to 1.0 for all the samples, and the distribution of weighted residual along the zero line.

Mass spectra were recorded using direct inlet probe. Analyses were performed with a Thermo Finnigan Trace MS Plus. The samples were dissolved in acetonitrile. Ionization occurred by EI mode with an electron energy at 70 eV.

Crystal Structure Analysis. A suitable crystal of $[Ru(tpy)(CO)_2TFA]^+[PF_6]^-$ was coated with Paratone N oil, suspended in a small fiber loop and placed in a cooled nitrogen gas stream at 173 K on a Bruker D8 SMART APEX CCD sealed tube diffractometer with graphite monochromated Mo Kα (0.71073 Å) radiation. Data were measured using a series of combinations of phi and omega scans with 10 s frame exposures and 0.3° frame widths. Data collection, indexing, and initial cell refinements were all carried out using[26] software. Frame integration and final cell refinements were done using SAINT[27] software. The final cell parameters were determined from least-squares refinement on 7157 reflections. The SADABS[28] program was used to carry out absorption corrections. The structure was solved using direct methods and difference Fourier techniques (SHELXTL, V6.12).[29] Hydrogen atoms were placed in their expected chemical positions using the HFIX command and were included in the final cycles of least-squares with isotropic U_{ij}'s related to the atom's ridden upon. All non-hydrogen atoms were refined anisotropically. Scattering factors and anomalous dispersion corrections are taken from the International Tables for X-ray Crystallography.[30] Structure solution, refinement, graphics, and generation of publication materials were performed by using SHELXTL, V6.12, software.

Computational Details. For geometry optimization and the ground state electronic structure calculations, the DFT method with the Becke,[31] three parameter hybrid functional and Lee−Yang−Parr's[32] gradient corrected correlation functional (B3LYP) was used. The calculations were performed with the Gaussian03 (G03)[33] program. The LanL2DZ basis set and effective core potential were used for the Ru atom and the 6-31G** basis sets were used for all other atoms, respectively. The nature of all stationary points was confirmed by performing a normal-mode analysis.

Solvent effects play an important role in the electronic structure of the Ru complexes.[34] The conductorlike polarizable continuum model method[35−37] (CPCM) with acetonitrile as solvent was used to calculate the electronic structure and the excited states of the complex in solution.

Time-dependent density functional theory[38,39] (TDDFT) calculations have provided excitation energies of Ru complexes that agree well with experiments.[40] In the Gaussian03 implementation of TDDFT, excitation energies are determined as poles of the response functions that were obtained from (Kohn−Sham) KS orbital energies and coupling matrix elements.[38] It involves calculating the KS orbitals and orbital energies as the first step followed by solving an eigenvalue problem to determine the poles.[38] The KS orbital energy difference of the orbitals relevant to the transition can be viewed as an approximation to the transition energy, and the TDDFT method adds to an correction of the Coulomb energy and the exchange and correlation (XC) energy because of the response of the electron density.

From the singlet ground state, optimized in the gas phase, thirty-two singlet excited states and the corresponding oscillator strengths have been determined with a TDDFT calculation using Gaussian03. The computational results are summarized in Table 1. The TDDFT calculation does not provide the electronic structures of the excited states; however, the electronic distribution and the localization of the singlet excited states may be visualized using the electron density difference maps (EDDMs).[41] GaussSum 1.0[42] was used for EDDMs calculations and for the electronic spectrum simulation. Only electronic transitions with an oscillator strength value (f) higher than 0.05 are reported. Triplet excited states were calculated either from the lowest-lying triplet state (T_1), optimized in the gas phase, or from the singlet ground state (S_0). The emission energies were calculated employing the ΔSCF approach,[43,44] as was the vertical energy gap between the S_0 and T_1 energies, both evaluated at the optimized geometry of T_1. The assignments of the triplet states were based on the major contributing excitations (when the transition coefficient of the major excitation is higher than the other coefficients by 0.2 or more). All DFT calculations on the free ligand tpy were performed at the B3LYP level with the 6-31G** basis set; acetonitrile was used as solvent for the TDDFT calculations.

For qualitative analysis and the emission spectra assignment, we calculated KS orbitals of both the singlet and triplet states of the dimer to examine the influence of intermolecular interactions on orbital energies and, subsequently, transition energies. We optimized the molecular geometry with the singlet ground state electronic configuration. Two such units are then placed together, and the distance between the two tpy surfaces are made to be 3 Å. The calculation was performed using SIESTA-2.0.1 package and revised

---

(26) *SMART Version 5.628*; Bruker AXS, Inc.: Madison, WI, 2003.
(27) *SAINT Version 6.36A*; Bruker AXS, Inc.: Madison, WI, 2002.
(28) Sheldrick, G. M. *SADABS Version 2.10*; University of Göttingen: Göttingen, Germany, 2003.
(29) *SHELXTL V6.12*; Bruker AXS, Inc.: Madison, WI, 2002.
(30) Wilson, A. J. C. *International Tables for X-ray Crystallography, Volume C*; Academic Publishers: Dordrecht, 1992; Tables 6.1.1.4 (pp 500−502) and 4.2.6.8 (pp 219−222).
(31) Becke, A. D. *J. Chem. Phys.* **1993**, *98*, 5648−5652.
(32) Lee, C.; Yang, W.; Parr, R. G. *Phys. Rev. B: Condens. Matter* **1988**, *37*, 785−789.
(33) Frisch, M. J.; Trucks, G. W.; Schlegel, H. B.; Scuseria, G. E.; Robb, M. A.; Cheeseman, J. R.; Montgomery, J. A., Jr.; Vreven, T.; Kudin, K. N.; Burant, J. C.; Millam, J. M.; Iyengar, S. S.; Tomasi, J.; Barone, V.; Mennucci, B.; Cossi, M.; Scalmani, G.; Rega, N.; Petersson, G. A.; Nakatsuji, H.; Hada, M.; Ehara, M.; Toyota, K.; Fukuda, R.; Hasegawa, J.; Ishida, M.; Nakajima, T.; Honda, Y.; Kitao, O.; Nakai, H.; Klene, M.; Li, X.; Knox, J. E.; Hratchian, H. P.; Cross, J. B.; Bakken, V.; Adamo, C.; Jaramillo, J.; Gomperts, R.; Stratmann, R. E.; Yazyev, O.; Austin, A. J.; Cammi, R.; Pomelli, C.; Ochterski, J. W.; Ayala, P. Y.; Morokuma, K.; Voth, G. A.; Salvador, P.; Dannenberg, J. J.; Zakrzewski, V. G.; Dapprich, S.; Daniels, A. D.; Strain, M. C.; Farkas, O.; Malick, D. K.; Rabuck, A. D.; Raghavachari, K.; Foresman, J. B.; Ortiz, J. V.; Cui, Q.; Baboul, A. G.; Clifford, S.; Cioslowski, J.; Stefanov, B. B.; Liu, G.; Liashenko, A.; Piskorz, P.; Komaromi, I.; Martin, R. L.; Fox, D. J.; Keith, T.; Al-Laham, M. A.; Peng, C. Y.; Nanayakkara, A.; Challacombe, M.; Gill, P. M. W.; Johnson, B.; Chen, W.; Wong, M. W.; Gonzalez, C.; Pople, J. A. *Gaussian 03*, revision C.02; Gaussian, Inc.: Wallingford, CT, 2004.
(34) Fantacci, S.; De Angelis, F.; Selloni, A. *J. Am. Chem. Soc.* **2003**, *125*, 4381−4387.
(35) Barone, V.; Cossi, M. *J. Phys. Chem. A* **1998**, *102*, 1995−2001.
(36) Cossi, M.; Barone, V. *J. Chem. Phys.* **2001**, *115*, 4708−4717.
(37) Cossi, M.; Rega, N.; Scalmani, G.; Barone, V. *J. Comput. Chem.* **2003**, *24*, 669−681.
(38) Stratmann, R. E.; Scuseria, G. E.; Frisch, M. J. *J. Chem. Phys.* **1998**, *109*, 8218−8224.
(39) Casida, M. E.; Jamorski, C.; Casida, K. C.; Salahub, D. R. *J. Chem. Phys.* **1998**, *108*, 4439−4449.
(40) De Angelis, F.; Fantacci, S.; Selloni, A. *Chem. Phys. Lett.* **2004**, *389*, 204−208.
(41) Browne, W. R.; O'Boyle, N. M.; McGarvey, J. J.; Vos, J. G. *Chem. Soc. Rev.* **2005**, *34*, 641−663.
(42) O'Boyle, N. M.; Vos, J. G. *GaussSum (1.0)*; Dublin City University: Dublin, 2005. Available at http://gausssum.sourceforge.net.
(43) Ziegler, T.; Rauk, A.; Baerends, E. J. *Theor. Chim. Acta* **1977**, *43*, 261−271.
(44) Daul, C. *Int. J. Quantum Chem.* **1994**, *52*, 867−877.

Table 1. Crystal Data and Structure Refinement for $[Ru(tpy)(CO)_2TFA]^+[PF_6]^-$

empirical formula	$C_{19}H_{11}F_9N_3O_4PRu$	
fw	648.35	
T	173(2) K	
wavelength	0.71073 Å	
cryst syst	triclinic	
space group	$P\bar{1}$	
unit cell dimensions	$a = 8.2573(5)$ Å	$\alpha = 75.376(1)°$
	$b = 9.9638(6)$ Å	$\beta = 85.504(1)°$
	$c = 14.4216(9)$ Å	$\gamma = 77.171(1)°$
V	$1119.11(12)$ Å^3	
Z	2	
density (calcd)	1.924 Mg/m^3	
abs coeff	0.881 mm^{-1}	
F(000)	636	
cryst size	$0.45 \times 0.27 \times 0.16$ mm^3	
θ range for data collection	1.46−28.29°	
Index ranges	$-11 \leq h \leq 10$	
	$-13 \leq k \leq 13$	
	$-19 \leq l \leq 19$	
reflns collected	15550	
indep reflns	5527 [*R*(int) = 0.0246]	
completeness to $\theta = 28.29°$	99.7%	
abs correction	semiempirical from equivalents	
max and min transm	0.8719 and 0.6927	
refinement method	full-matrix least-squares on F^2	
data/restraints/params	5527/0/334	
GOF on F^2	1.043	
final *R* indices [$I > 2\sigma(I)$]	R1 = 0.0345, wR2 = 0.0898	
R indices (all data)	R1 = 0.0373, wR2 = 0.0916	
largest diff. peak and hole	0.925 and −0.678 e Å^{-3}	

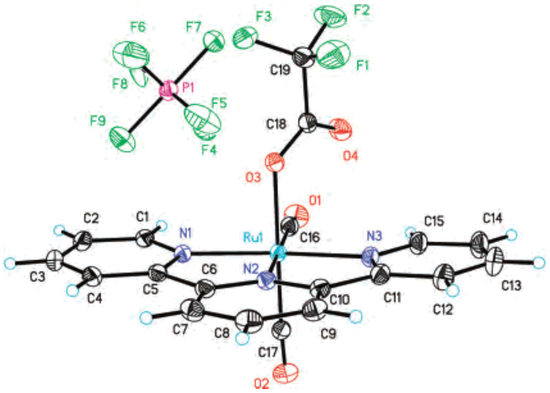

Figure 1. X-ray structure of $[Ru(tpy)(CO)_2TFA]^+[PF_6]^-$ showing the adopted labeling scheme, with displacement ellipsoid drawn at 30% probability.

PBE [45] XC potential. For Ru, we used a Troullier−Martins [46] type of pseudopotential with the relativistic effects included and a semicore. The reference valence configuration is $4s^24p^64d^74f^0$. For all the other atoms, we used double ζ[47] pseudoatomic orbital bases[48] and the Troullier−Martins[46] type of pseudopotential.

Synthesis of $K^+[Ru(TFA)_3(CO)_3]^-$. This compound was previously reported by Fachinetti and co-workers.[49] Herein, we report an alternative and higher yield preparation we have never published.[50]

After 300 mg of K_2CO_3 is dissolved in 10 mL of trifluoroacetic acid, $Ru_3(CO)_{12}$ (440 mg) is added. The bright orange solution is refluxed under N_2 for approximately 24 h, giving a pale yellow solution. The reaction mixture is cooled to room temperature, and then, the trifluoroacetic acid is evaporated by bubbling nitrogen through the solution. A yellow precipitate is collected after addition of diethyl ether (yield 87%, 1.012 g). ν_{co} (powder-ATR): 2149, 2078, 2041, 1668 cm^{-1}. Elemental analysis calculated for $C_9F_9O_9RuK$: %C 19.19. Found: %C 19.35.

Synthesis of $[Ru(tpy)(CO)_2TFA]^+[PF_6]^-$ (1). $K^+[Ru(CO)_3(TFA)_3]^-$ (200 mg) is dissolved in absolute ethanol, and 2,2′:6′,2″-terpyridine (83 mg) is added. The reaction mixture is refluxed under nitrogen for 2 h; rapid changes in the solution color (from violet to brown) are observed. The final dark-brown solution is cooled, and a black precipitate is collected by addition of a NH_4PF_6 aqueous solution. After filtration, the solid is washed with diethyl ether and dried (yield 45%, 109 mg). ν_{co} (powder-ATR): 2080, 2026, 1702 cm^{-1}. ^{1}H NMR (acetone-d_6, ppm): 9.07 (d, 2H), 8.87 (d, 2H), 8.81 (d, 2H), 8.75 (t, 1H), 8.47 (t, 2H), 7.90 (t, 2H). ^{13}C NMR (acetone-d_6, ppm): 194.8 (CF_3*CO*), 193.5, 189.7, 158.2, 157.3, 155.0, 143.0, 141.7, 129.1, 125.7, 124.6, 115.2 (CF_3, 291.3 Hz). MS: *m*/*z* 504 (M^+), *m*/*z* 476 ($M^+ - CO$). Elemental analysis calculated for $C_{19}H_{11}F_9N_3O_4PRu$: %C 35.20, %H 1.71, %N 6.48. Found: %C 35.09, %H 1.73 %N 6.35.

Results and Discussion

The terpyridine ruthenium complex $[Ru(tpy)(CO)_2Cl]^+[PF_6]^-$ has been prepared in good yield from $[Ru(CO)_2Cl_2]_n$ in refluxing EtOH/H_2O.[20,21] In an attempt to find a more reactive ruthenium-carbonyl containing complex for more selective ligand substitutions, we have been studying the reactivity of $K^+[Ru(CO)_3(TFA)_3]^-$ with a wide range of diimine and triimine ligands.[51] The analogous complex $[Ru(tpy)(CO)_2TFA]^+[PF_6]^-$ (**1**) was obtained in moderate yield, and during the progress of the reaction, several rapid color changes were observed which we associated with the well-known η^2 to η^3 conversion previously observed for related terpyridine complexes.[52,53] We therefore undertook an NMR study at ambient temperatures to investigate the overall pathway for progressive ligand substitution on the starting $K^+[Ru(CO)_3(TFA)_3]^-$ in methanol (see Supporting information).

X-ray Structure. The solid-state structure of $[Ru(tpy)(CO)_2(TFA)]^+[PF_6]^-$ is shown in Figure 1, and crystal data are given in Table 1. Selected experimental X-ray and computed bond distances and angles are reported in Table 2. Ru(II)-tpy derivatives are characterized by a pseudo-octahedral coordination of the metal center. The bite angle of tpy is significantly smaller than the ideally required 180°. For example, Collin and co-workers[54] reported a bite angle

---

(45) Zhang, Y. K.; Yang, W. T. *Phys. Rev. Lett.* **1998**, *80*, 890.

(46) Troullier, N.; Martins, J. L. *Phys. Rev. B* **1991**, *43*, 8861−8869.

(47) SanchezPortal, D.; Artacho, E.; Soler, J. M. *J. Phys.: Condens. Matter* **1996**, *8*, 3859−3880.

(48) Sankey, O. F.; Niklewski, D. J. *Phys. Rev. B* **1989**, *40*, 3979−3995.

(49) Fachinetti, G.; Funaioli, T.; Lecci, L.; Marchetti, F. *Inorg. Chem.* **1996**, *35*, 7217−7224.

(50) Skinner, M. D. California State University, 1986.

(51) Rosenberg, E., Ross, J. B. A., Sharmin, A., Minazzo, A., Gobetto, R., Nervi, C., Salassa, L., Garino, C. New Luminescent Ruthenium Probes For Bioconjugation: Tuning Photophisical Properties With π-Acid Ligands. Presented at the Third International Symposium on Bioorganometallic Chemistry, Milan, July 2006; abstract 44.

(52) Gellin, A.; Orrell, K. G.; Osborne, A. G.; Šik, V. *J. Chem. Soc., Dalton Trans*. **1998**, *6*, 937−945.

(53) Deacon, G. B.; Patrick, J. M.; Skelton, B. W.; Thomas, N. C.; White, A. H. *Aust. J. Chem.* **1984**, *37*, 929−936.

(54) Bonnet, S.; Collin, J. P.; Gruber, N.; Sauvage, J. P.; Schofield, E. R. *J. Chem. Soc., Dalton. Trans.* **2003**, 4654−4662.

Table 2. Selected Bond Distances (Å) and Angles (deg) of $[Ru(tpy)(CO)_2(TFA)]^+$ on Calculated Singlet Ground and Lowest-Lying Triplet State Geometries and X-ray Crystallography

	Ru−N2	Ru−N3	Ru−N1	Ru−C16	Ru−C17	Ru−O3	C16−Ru−C17	N1−Ru−N3
X−ray	2.0160 (19)	2.092 (2)	2.0920 (19)	1.935 (3)	1.874 (3)	2.1091 (17)	85.91 (10)	156.89 (8)
singlet	2.04	2.13	2.14	1.96	1.92	2.10	90.96	156.43
triplet	2.03	2.14	2.10	1.97	1.93	2.09	91.17	157.00

smaller than 160° for tpy. Similarly, **1** displays a N_1−Ru−N_3 angle of 156.89(8)°. Furthermore, the Ru−N(1) and Ru−N(3) distances between the metal center and the outer pyridine rings are longer (2.092(19) and 2.092(2) Å) than the Ru−N(2) distance (2.0160(19) Å).

There is a small difference in length between the two Ru−C(O) bonds: C(16) is at 1.935(3) Å from the metal atom, while the other, C(17), is placed at 1.874(3) Å. The Ru−O distance (2.1091(17) Å) is close to the values of Ru−O bonds reported for the complex $K^+[Ru(TFA)_3(CO)_3]^-$ by Fachinetti et al.[49]

The crystal packing of **1** is driven by ionic forces between the positively charged ruthenium-containing moiety and the negative PF_6^- anions. In addition, two different kinds of weak intermolecular interactions are present. Intermolecular $\pi-\pi$ stacking interaction of tpy aromatic rings is one of these forces in the solid state, along with weak contacts between tpy C−H groups and polar groups of the coordinated TFA (there has been discussion on the nature and definition of these interactions: hydrogen bond, van der Waals interactions).[55−57]

Selected contact distances are represented for both kinds of interaction in Figure 2. The shortest distance retrieved between stacked aromatic rings is 3.48 Å.

As shown by spectroscopic data, these weak interactions play an important role in the fluorescent properties of the complex (vide infra).

DFT Optimized Structures. Geometric parameters for **1** optimized in the ground-state configuration and in the lowest-lying triplet configuration are summarized in Table 2. Bond lengths and angles of the singlet ground-state geometry are in good agreement with the X-ray values. Ru−N lengths are slightly overestimated (about 0.02−0.04 Å). The same trend is observed for Ru−C bonds, where the difference is 0.03 Å for Ru−C(16) and 0.01 Å for Ru−C(17). The tpy bite angle determined computationally is 156.4°, close to the X-ray experimental value (156.9°). In the lowest-lying triplet state, critical bond distances remain almost unchanged except for the Ru−N(1) distance, where the bond decreases to 2.10 Å. Consequently, a slightly higher tpy bite angle is found (157.2°). The weak coordination of tpy can be related to the independence of these geometric parameters from the electronic structure of the complex.

The free ligand terpyridine was optimized in two ground-state conformations; the first is the most stable planar *trans*−*trans*, reported by Bessel[58] in a X-ray diffraction study, and the latter is a distorted *cis*−*cis* conformation obtained by starting the optimization calculation from the planar *cis*−*cis* structure. *Trans-trans* tpy is coplanar and symmetrical (a distortion of 7.2° is reported in the solid-state structure). Nitrogen atoms on the lateral pyridines are at 2.45 Å from the hydrogens in the *meta* position of the central ring. The central nitrogen shows an intramolecular distance of 2.48 Å with the closest hydrogen on the other rings.

In the distorted *cis*−*cis* structure, the two lateral pyridine rings are rotated both in the same direction by 35.9°. The angle defined by the three nitrogen atoms is 118.5°.

Molecular Orbital Analysis. The electronic structure of $[Ru(tpy)(CO)_2(TFA)]^+$ has distinct features in vacuo and in acetonitrile. Since acetonitrile is more relevant in our synthesis and spectroscopy study, we discuss in detail the molecular orbitals of complex **1** in acetonitrile. Here, the two highest occupied molecular orbitals have a high tpy character (57% each) and a reduced metal character, 33% for the HOMO and 25% for the HOMO−1, which has also a higher TFA contribution (14% instead of 6%). The energy difference between them is of 0.22 eV (1774 cm^{-1}), and they are involved in the two electronic transition in the absorption spectrum at the lowest energies. Both these orbitals display a backbonding contribution to either CO_{ax} (in-phase, π CO orbitals) or TFA (out-of-phase, π^* TFA orbitals). The orbital HOMO−3 has a reduced ligand character (30%) and a higher metal one (49%), while HOMO−4 is mainly TFA (60%) centered. HOMO−5 is practically a pure π tpy orbital, and the next three orbitals at lower energy are TFA- and tpy-based.

The LUMO has 94% tpy character and an energy gap with the HOMO of 4.26 eV (34.4×10^3 cm^{-1}). An interesting feature of this orbital is the presence of delocalization from tpy to the CO_{eq} (*trans* to tpy) through a π orbital localized onto the ancillary ligand. Furthermore, a σ Ru−O interaction is observed in the LUMO (Figure 3). The next three higher

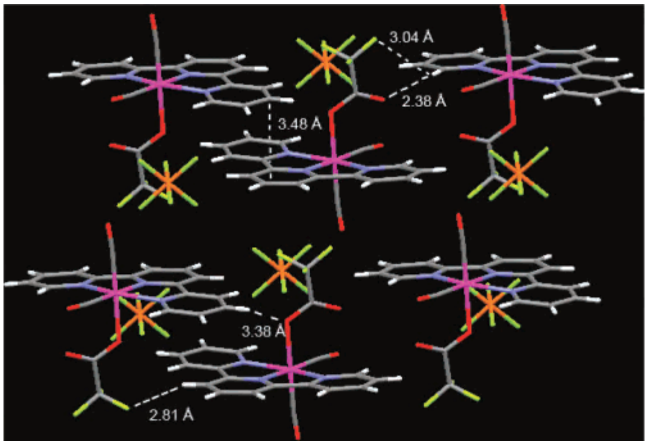

Figure 2. Crystal packing of $[Ru(tpy)(CO)_2TFA]^+[PF_6]^-$.

---

(55) Aime, S.; Diana, E.; Gobetto, R.; Milanesio, M.; Valls, E.; Viterbo, D. *Organometallics* **2002**, *21*, 50−57.
(56) Orlova, G.; Scheiner, S. *J. Phys. Chem. A* **1998**, *102*, 260−269.
(57) Scheiner, S.; Kar, T. *J. Phys. Chem. A* **2002**, *106*, 1784−1789.
(58) Bessel, C. A.; See, R. F.; Jameson, D. L.; Churchill, M. R.; Takeuchi, K. J. *J. Chem. Soc., Dalton Trans.* **1992**, 3223−3228.

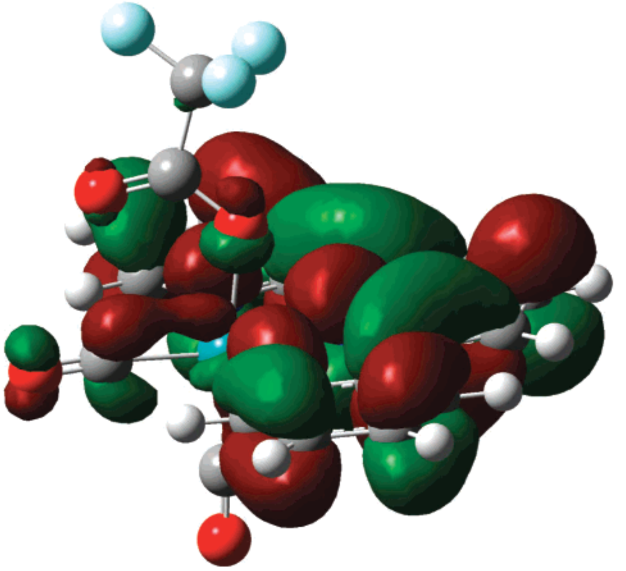

Figure 3. LUMO representation for [Ru(tpy)(CO)$_2$TFA]$^+$[PF$_6$]$^-$.

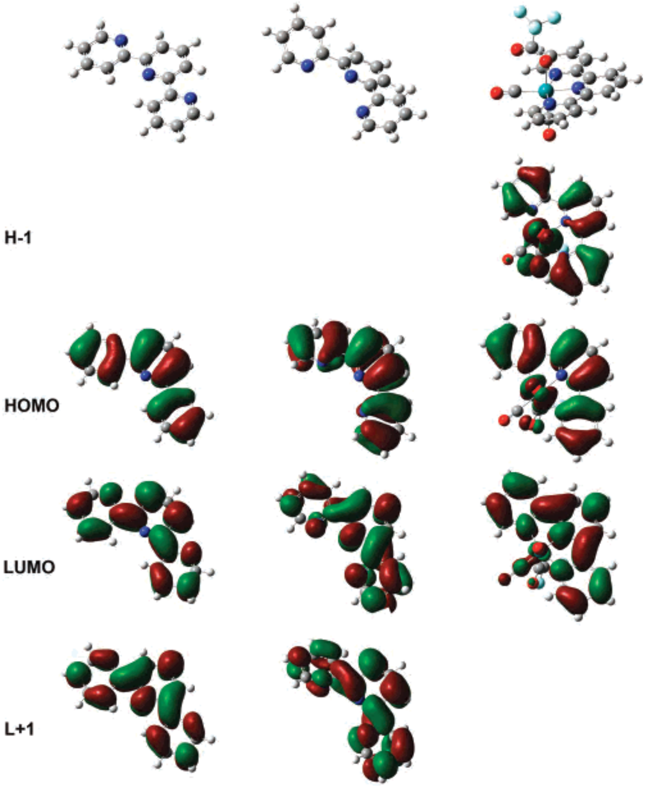

Figure 4. Schematic diagram of selected frontier orbitals for *trans*−*trans* tpy, *cis*−*cis* tpy, and [Ru(tpy)(CO)$_2$TFA]$^+$[PF$_6$]$^-$.

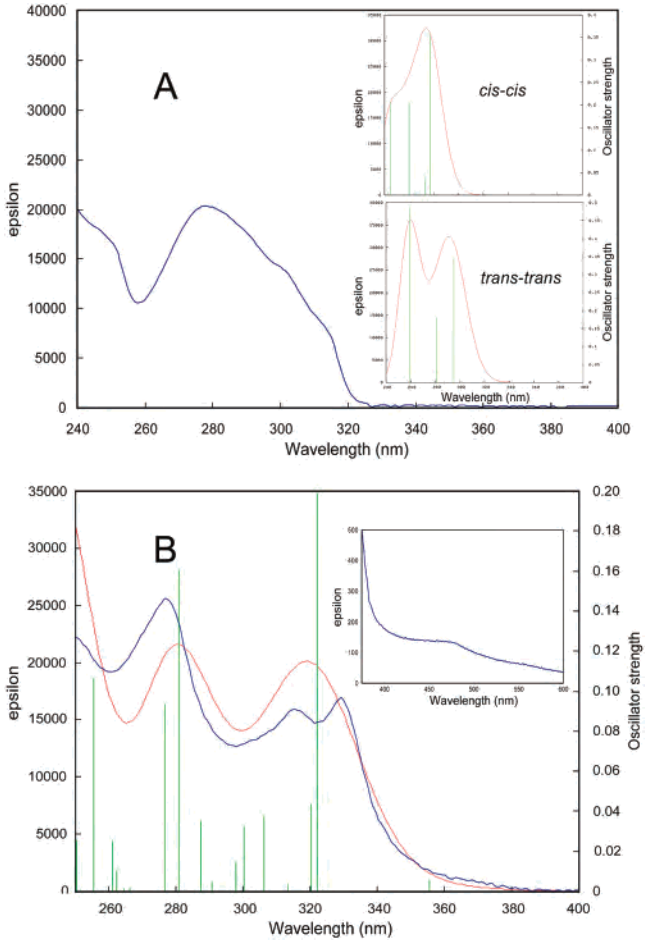

Figure 5. Calculated (red line) and experimental (blue line) absorption spectra for tpy (A) and [Ru(tpy)(CO)$_2$TFA]$^+$[PF$_6$]$^-$ (B) in acetonitrile. B inset: zoom of the region between 375 and 600 nm for a 10^{-4} M solution of [Ru(tpy)(CO)$_2$TFA]$^+$[PF$_6$]$^-$ in acetonitrile. Theoretical curves were obtained using the program GAUSSSUM 1.0. The excited states are shown as vertical bars with height equal to the extinction coefficient.

energy LUMOs all have more than 95% tpy character.[59] Orbitals with a mixed metal-carbonyl character are found at still higher energy after this set of unoccupied orbitals. Selected orbitals for **1**, *trans*−*trans* tpy and *cis*−*cis* tpy, are depicted in Figure 4.

The HOMO orbitals for the two tpy conformations have the same shape despite their different geometries. Their energies are almost equal with the *cis*−*cis* being 0.006 eV (48 cm^{-1}) more stable. In this conformation, LUMO and LUMO+1 are energetically degenerate, while in the *trans*−*trans* tpy there is an energy difference of 0.003 eV (24 cm^{-1}). Rotation of the lateral rings does not affect the nature of these unoccupied molecular orbitals (except for some distortion), and they have the same shape for the two different computed structure.

Electronic Absorption Spectra and Singlet Excited States. The absorption spectra for free tpy and [Ru(tpy)(CO)$_2$TFA]$^+$[PF$_6$]$^-$ were measured in acetonitrile. Results and assignments based on the computational data are reported in Table 3. Figure 5 compares the experimental and theoretical absorption spectra. The latter were calculated employing the freeware program GaussSum.[42]

The experimental UV−vis spectra of tpy shows two absorptions peaks, one at 232 nm (not shown) and another at about 276 nm. The computed singlet transition energies, both for *trans*−*trans* and for *cis*−*cis* tpy, follow the trends of the experimental data. However, in the case of *trans*−*trans* tpy, the transition energies are underestimated. The higher energy band has mixed composition with a major $\pi-\pi^*$ contribution (S1a, 259 nm), whereas the two transitions at lower energies (S1b, 281, and S1c, 295 nm) account

---

(59) Vlček, A., Jr. *Coord. Chem. Rev.* **2002**, *230*, 225−242.

Table 3. Experimental Electronic Transition and Calculated Singlet Excited States of tpy and $[Ru(tpy)(CO)_2(TFA)]^+$

compd	E_{exp}, 10^3 cm^{-1} (ϵ, M^{-1} cm^{-1})	λ_{max} (nm)	E_{calc}, 10^3 cm^{-1} (nm)	f	major contribution	character
trans−trans tpy	43.1 (20900)	232	**S1a:** 38.6 (259)	0.49	HOMO−2 → LUMO (65%)	$\pi-\pi^*$
	36.2 (20200)	276	**S1b:** 35.6 (281)	0.18	HOMO → LUMO (84%)	$\pi-\pi^*$
			S1c: 33.9 (295)	0.35	HOMO → LUMO+1 (88%)	$\pi-\pi^*$
cis−cis tpy			**S2a:** 40.8 (245)	0.21	HOMO−3 → LUMO+1 (55%)	$\pi-\pi^*$
			S2b: 38.5 (260)	0.20	HOMO → LUMO+1 (83%)	$\pi-\pi^*$
			S2c: 36.1 (277)	0.35	HOMO → LUMO (80%)	$\pi-\pi^*$
1	36.0 (25700)	278	**S3a:** 36.2 (276)	0.09	HOMO−3 → LUMO+1 (74%)	Ru,tpy → tpy
			S3b: 35.6 (281)	0.16	HOMO−3 → LUMO+1 (16%) HOMO−1 → LUMO+1 (32%) HOMO → LUMO+1 (28%)	Ru,tpy → tpy
	31.6 (16300)	323	**S3c:** 31.0 (321)	0.20	HOMO → LUMO (11%) HOMO−1 → LUMO (68%)	Ru,tpy → tpy

for the experimental absorption band with its maximum at 276 nm. These latter transitions are $\pi-\pi^*$ and are characterized by almost pure one-electron transfers from the partially bonding HOMO to the LUMO or the LUMO+1, respectively. The oscillator strength values of the three main electronic transitions are in good agreement with the experimental extinction coefficients. In spite of different structures, the computed excited states for *cis−cis* tpy and *trans−trans* tpy are similar. However, the results for *cis−cis* tpy match the experimental data better. Interestingly, the energies of the S2b (260 nm) and S2c (277 nm) transitions are switched with respect to the corresponding values at lower energies of the *trans−trans* conformer. This is due to the energy degeneration of the LUMO and LUMO+1 orbitals.

The $[Ru(tpy)(CO)_2TFA]^+[PF_6]^-$ absorption slightly differs from that of tpy. There is a red shift of all bands, and the band at 323 nm is split as a result of vibrational coupling. The diimine ligand is perturbed by metal coordination, but it is possible to recognize the same characteristics for the electronic transition of the two free ligand species. The assignments in Table 3 and the EDDMs[42] presented in Figure 6 show the close similarity of the absorption bands of these different systems. The calculations indicate a metal contribution in the case of the complex (contributions to HOMO−1 orbital are 25% metal orbitals and 57% tpy π); there is also a significant contribution form the TFA group. These contributions are consistent with the red shift of the absorption bands. The electronic transitions S1b and S2b of the two tpy conformers are absent in the case of the complex.

The band at 278 nm can be attributed to tpy-centered transitions (S3a and S3b), where the metal contribution is greater and some TFA contribution is also present. Interestingly, no classical metal-to-ligand charge-transfer bands are present in the visible region. The closest electronic transition of that kind is the S3a transition. It has the characteristics of an MLLCT, but it is located in the UV region of the spectrum. The oscillator strength values are in good agreement with the relative intensities of the experimental bands.

The absorption spectrum of $[Ru(tpy)(CO)_2TFA]^+[PF_6]^-$ does not show concentration-dependent features, but it must be pointed out that a very weak band appears around 470 nm (Figure 5C) in concentrated solutions (10^{-4} M). This band is related to the formation of ground-state dimeric (or oligomeric) species, as observed also in the emission spectra recorded at 77 K.

Solution and Solid-State Luminescence Properties of tpy. To understand the nature of the emission properties of the complex, we studied the emission properties of tpy at different concentrations (ranging from 10^{-8} to 10^{-4} M) and different temperatures (77 K and RT). The tpy emission spectrum with excitation at 275 nm at different concentrations in acetonitrile glass (77 K) is reported in Figure 7a. At low concentration, the band centered at 440 nm (22.7×10^3 cm^{-1}) is slightly structured and has a vibrational profile which corresponds to the C═C and C═N stretching modes (FWMH $\sim$ 1300 cm^{-1}). The short lifetime (see Table 4) and the presence of the same band at room temperature (Figure 7b) suggests a $^1\pi-\pi^*$ assignment for this transition. As the

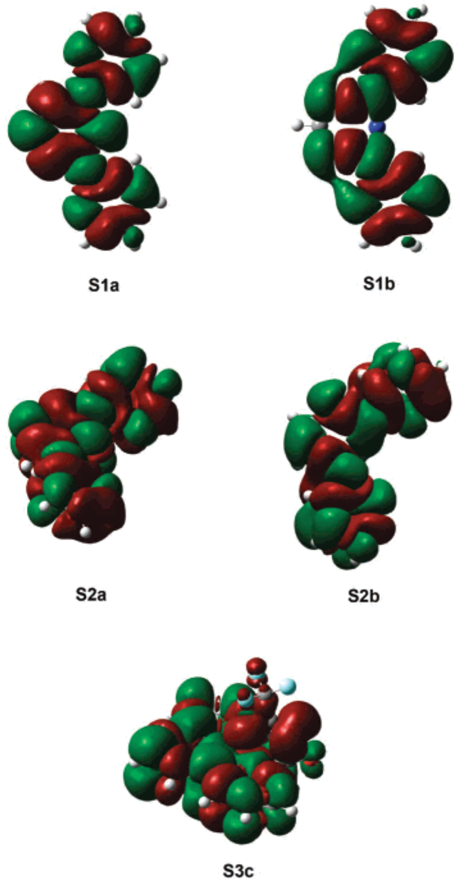

Figure 6. Electron density difference maps (EDDMs) of the lowest energy singlet electronic transition of *trans−trans* tpy (S1b and S1c), *cis−cis* tpy (S2b and S2c), and $[Ru(tpy)(CO)_2TFA]^+[PF_6]^-$ (S3c). Red indicates a decrease in charge density, while green indicates an increase.

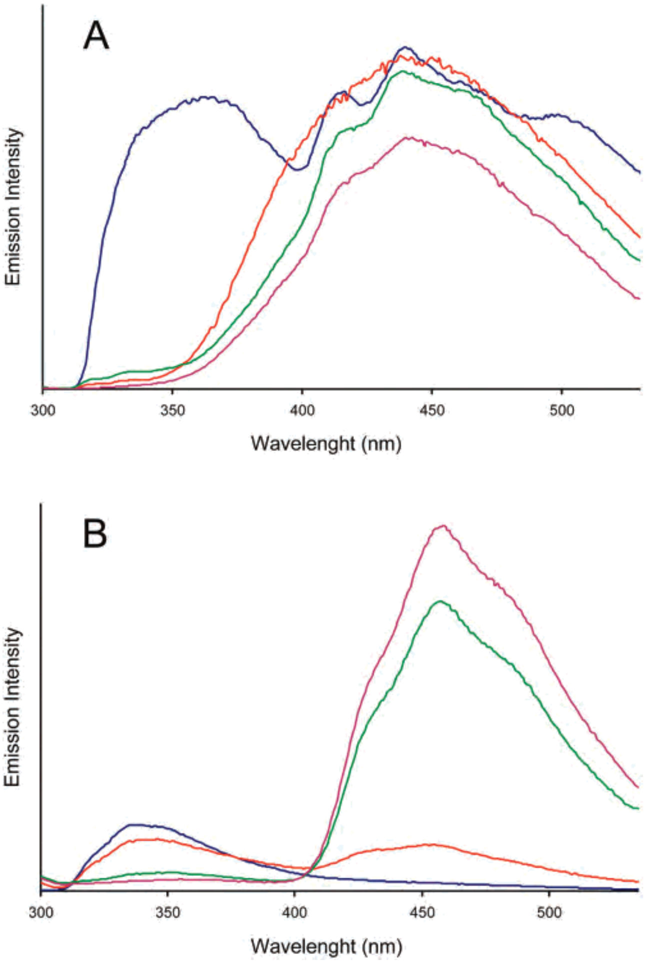

Figure 7. Concentration dependence of the emission spectrum of tpy in acetonitrile at 77 K (A) and at room temperature (B); blue line 1 × 10^{-4} M, red line 5 × 10^{-6} M, green line 5 × 10^{-7} M, violet line 5 × 10^{-8} M. Excitation wavelength is 275 nm. Low-temperature spectra were normalized.

concentration is increased, a shoulder at 501 nm (20.0 × 10^3 cm^{-1}) and a band at about 360 nm (27.8 × 10^3 cm^{-1}) appear. The first band can be related to $\pi-\pi$ stacking[15] due to the formation of dimeric (or oligomeric) excimerlike structures. The origin of the second band can be rationalized by using data published in the literature combined with computational results. Electronic spectroscopy studies on the pH-dependent conformations of tpy were published in the 1960s and 1970s.[60,61] They showed a deprotonated monomer singlet emission centered at around 450 nm (this band was also present in organic solvents with low polarity), and a structureless large band originating from the monoprotonated tpy located at 370 nm. The first transition was associated with a *trans*−*trans* conformation of tpy, and the second with a *cis*−*trans* conformation. A third low-energy transition was associated with a *cis*−*cis* conformation and a deprotonated form of the ligand. According to our calculation, however, the conformer at highest energy is the *cis*−*cis*. This result is supported by the singlet excited-state calculation on the *cis*−*trans* tpy (not shown) where all transitions are shifted to lower energies. Furthermore, there is a similarity between the band at 360 nm and highest energy transition of the ruthenium complex, where the ligand is constrained in a *cis*−*cis* conformation. It is beyond the scope of this work to explore the possible tpy conformational changes in the excited state, but it seems evident from the data collected that this process is related to the formation of one or more types of dimers (oligomers). Partially $\pi-\pi$ stacked structures containing tpy units with *cis*−*cis* conformation can be responsible for the emission band at 360 nm. Furthermore, at room temperature it is possible to observe at least three species in the solid-state emission spectrum (Figure 8) of tpy: the dimer (or oligomer) complex at 520 nm (19.2 × 10^3 cm^{-1}); the *trans*−*trans* tpy monomer at 460 nm (21.7 × 10^3 cm^{-1}); and finally the *cis*−*cis* tpy monomer at 370 nm (27.0 × 10^3 cm^{-1}).

Table 4. Luminescence Lifetime of tpy and $[Ru(tpy)(CO)_2TFA]^+[PF_6]^-$ in Acetonitrile

	77 K		RT	
	λ_{max}	τ	λ_{max}	τ
tpy	370 nm	$\tau_1 = 1.5$ ns $\tau_2 = 5.5$ ns	345 nm	$\tau < 1$ ns
	440 nm	$\tau_1 = 4.8$ ns $\tau_2 = 13.9$ ns	460 nm	$\tau = 8.2$ ns
1	485 nm	$\tau > 50\ \mu s^a$	351 nm	$\tau = 9.5$ ns
	520 nm	$\tau > 50\ \mu s^a$		
	603 nm	$\tau \sim 10\ \mu s$		

[a] Due to the nano-led repetition rate maximum measurable lifetime is about 50 μs.

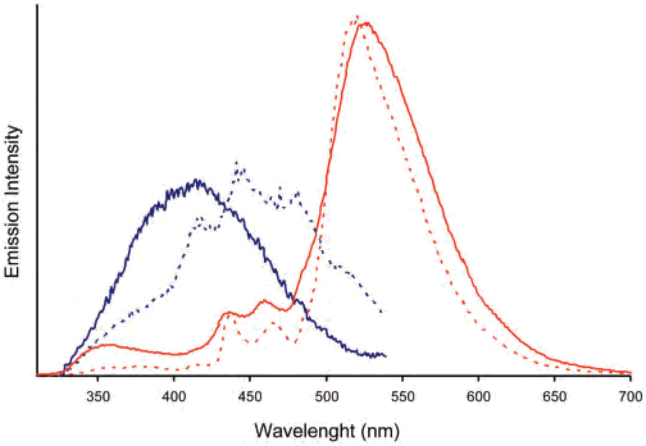

Figure 8. Solid-state emission spectra of tpy at 77 K (dashed red line) and room temperature (solid red line), and of $[Ru(tpy)(CO)_2TFA]^+[PF_6]^-$ at 77 K (dashed blue line) and room temperature (solid blue line).

Room-temperature spectra recorded in different polarity solvents and at different concentrations confirm this interpretation. In acetonitrile (3.9 D), the band attributed to the dimer (oligomer) is not present even at high concentrations, while in methylene chloride (1.6 D) this band is evident upon excitation at 275 nm. At high concentrations of tpy in the latter solvent, an intense emission band due to the *cis*−*cis* isomer is also observed in the expected region. However, in acetonitrile the *cis*−*cis* conformations are present despite the solvent polarity. *Trans-trans* tpy is the dominant species at low concentration in acetonitrile, but the presence of a low-intensity band for *cis*−*cis* tpy (room temperature, Figure 7b) may indicate that some rearrangement also occurs in the tpy monomers when in the excited state. The change in peak

---

(60) Fink, D. W.; Ohnesorge, W. E. *J. Phys. Chem.* **1970**, *74*, 72−77.
(61) Nakamoto, K. *J. Phys. Chem.* **1960**, *64*, 1420−1425.

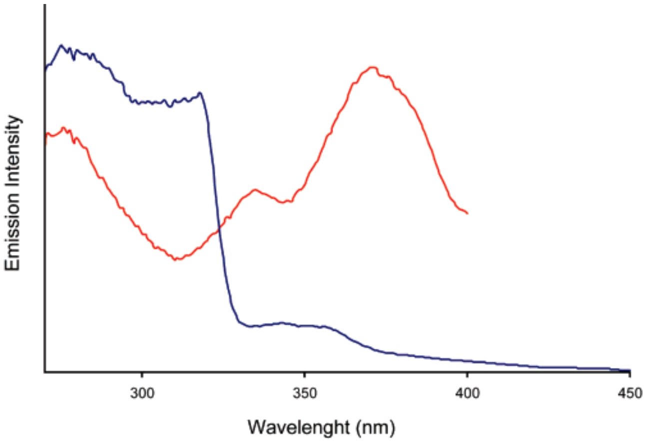

Figure 9. Excitation spectra of tpy in acetonitrile at 77 K monitoring emission at 510 nm (solid blue line) and at room temperature monitoring emission at 455 nm (solid red line).

ratio observed by increasing the concentration suggests that $\pi-\pi$ stacking may play a role in the process. Weak dimers (oligomers) containing tpy units with a *cis*−*cis* orientation are more likely at higher concentrations. The aggregates in solution are usually considered to be excimers, but ground-state complexes are implicated in the emission from rigid glasses. The absence of excimer band at room temperature indicates the low stability of the aggregate species, which probably dissociate and give monomer emissions.

All of these species have singlet character and short lifetimes (Table 4), whether at room temperature or low temperature.

The excitation spectra of tpy support this interpretation (Figure 9). At 77 K and high concentration (10^{-4} M), an excitation maximum centered at 350 (28.6×10^3 cm^{-1}) nm is present for the dimer band at 501 nm (20.0×10^3 cm^{-1}). Selective excitation at this wavelength causes a significant increase in the band intensity. Mixing contributions from the other bands of the emission spectra are present because of the spectral overlap. This peak at 350 nm disappears (a broad excitation band remains) when the concentration is less than micromolar levels, and only the 275 nm peak is present.

When monitoring the emission at 460 nm (21.7×10^3 cm^{-1}) at room temperature and high concentration of tpy, there are three bands in the excitation spectrum: 275, 345, and 375 nm. Surprisingly, the first has a low extinction coefficient compared to the other two bands. Decreasing the concentration causes an increase of the relative intensity of this band. The other two maxima can be reasonably assigned to dimeric (oligomeric) species or conformers. The different relative abundance of the various species, as well as their different extinction coefficients, are consistent with the excitation spectra. In the case of excimerlike species, the extinction should be very small (10 M^{-1} cm^{-1}).[15]

Solution and Solid-State Luminescence Properties of [Ru(tpy)(CO)$_2$TFA]$^+$[PF$_6$]$^-$. Complex **1** displays concentration-dependent luminescence features both at room temperature and a 77 K, in the glassy state. Some of these features are similar to those of the free ligand, but others are the result of an intermolecular ground-state interaction, such as tpy $\pi-\pi$ stacking or weak hydrogen bond contacts between two different metal complex molecules (Figure 2). The emission spectra for the complex were recorded at different concentrations, ranging from 10^{-6} to 10^{-3} M. Figure 10a shows emission spectra recorded at 77 K in acetonitrile glass, exciting at 330 nm. At low concentration, two major peaks appear at 452 nm (22.1×10^{-3} cm^{-1}) and at 485 nm (20.6×10^{-3} cm^{-1}); they can be assigned to a metal perturbed ^{3}LC ($^3\pi-\pi^*$) transition with resolved vibrational progression. The peak separation is about 1500 cm^{-1}, which corresponds to the C═C and C═N stretching modes; the emission lifetime of this band is longer than 50 μs (Table 4) indicating that no high-energy ^{3}MLCT states are mixing with this ligand-centered state. Two shoulders are resolved at 520 nm (19.2×10^{-3} cm^{-1}) and 559 nm (17.9×10^{-3} cm^{-1}), and a weak band can be observed at about 603 nm (16.6×10^{-3} cm^{-1}). Increasing the concentration of the complex solution causes a significant increase in the relative intensity of the 603 nm transition. This band becomes the most intense at millimolar concentrations of complex. The shoulder at 520 nm does not seem to be affected by concentration, while the one at 559 nm disappears or becomes covered by the tail of the low-energy band. These two bands were previously[15−17]

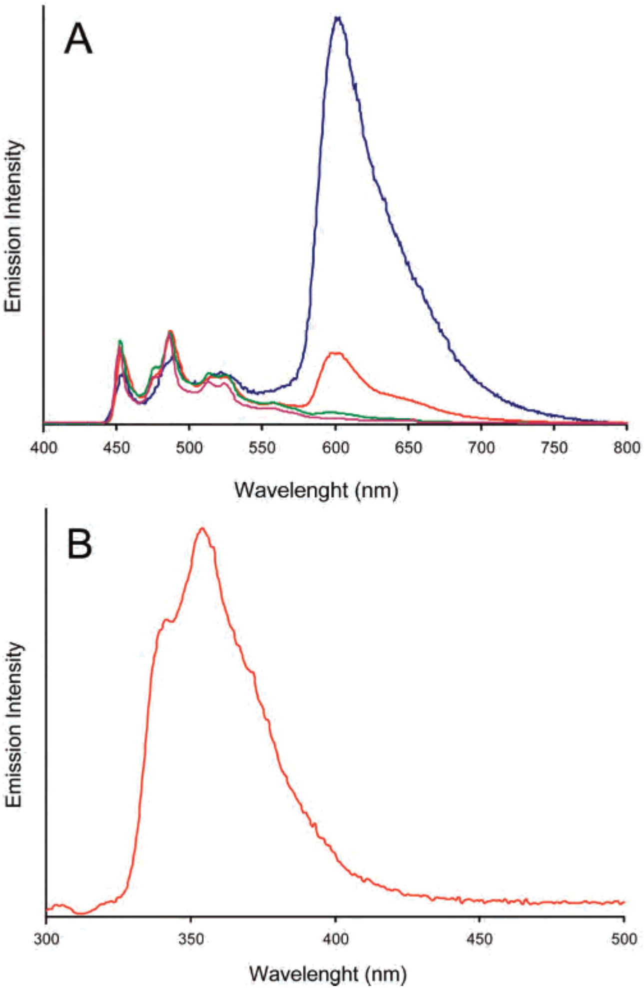

Figure 10. Concentration dependence of the emission spectrum of [Ru(tpy)(CO)$_2$TFA]$^+$[PF$_6$]$^-$ in acetonitrile at 77 K (A) and at room temperature (B); blue line 1×10^{-3} M, red line 1×10^{-4} M, green line 1×10^{-5} M, violet line 1×10^{-6} M. Low-temperature spectra were normalized.

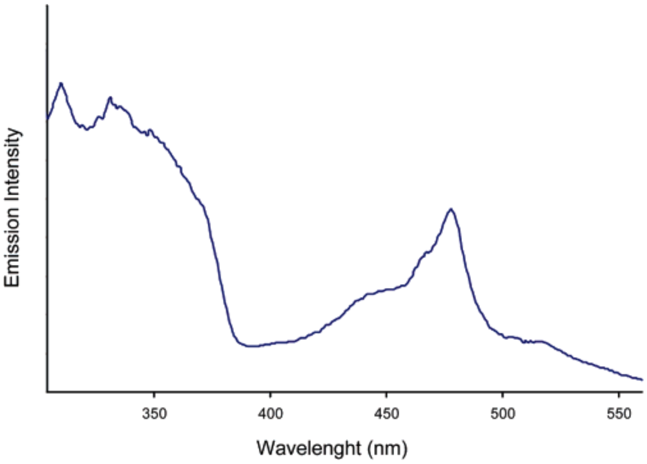

Figure 11. Excitation spectra (77 K) of [Ru(tpy)(CO)$_2$TFA]$^+$[PF$_6$]$^-$ monitoring emission at 603 nm in acetonitrile.

assigned to excimeric species originated by partial $\pi-\pi$ stacking of the tpy rings. The low intensity of these emission bands with respect of the dominant emission at 603 nm can be explained on assuming lower quantum yields for these species. However, oligomers with different geometries exist and compete in solution. For this reason, more stable aggregates are more abundant.

Interestingly, no band is observed in the 600 nm region for tpy at 77 K. Therefore, we considered that the metal has a role in the lowest-energy transition of the complex. The excitation spectrum (Figure 11) of the above-mentioned band of **1** shows a maximum at 470 nm (as well as the 10^{-4} M absorption spectrum), and excitation at this wavelength (77 K) gives intense emission at 603 nm. The width of this structureless band is 1300 cm^{-1} which suggests that a mixed excited-state transition could be responsible for this emission. In fact, the increase in intensity of this band accompanying the increase in concentration and the intermediate lifetime (around 10 μs) further support that a mixing between tpy-centered and metal-centered states is occurring. This is consistent with the data reported in the literature for square planar platinum complexes.[15-17] Further insights on the nature of this band are reported in the next sections.

At room temperature, [Ru(tpy)(CO)$_2$TFA]$^+$[PF$_6$]$^-$ has an emission band at 351 nm (28.5×10^{-3} cm^{-1}), which corresponds to the metal-perturbed ligand-centered singlet state.

Complex **1** displays only a single emission band in the solid state at room temperature (Figure 8). This electronic transition can be assigned to the singlet ligand-centered state. At 77 K in the solid state, the band at 441 nm (22.7×10^{-3} cm^{-1}) can be reasonably assigned to a metal-pertubated $^3\pi-\pi^*$ state, but dimeric (or oligomeric) species are likely present because a shoulder appears at around 510 nm (19.6×10^{-3} cm^{-1}). A band at 600 nm is visible when a 470 nm excitation light is employed, supporting this conclusion.

Triplet Excited States. Four triplet excited states were calculated both for *trans*−*trans* tpy and *cis*−*cis* tpy in acetonitrile solution using Gaussian03. The ground-state geometry was employed in this TDDFT calculation, as well as the CPCM method.[35-37] Since no phosphorescence is observed for the free ligand either at room temperature or at 77 K, we only comment here on the lowest-lying triplet state of the distorted *cis*−*cis* tpy. This state lies 381 nm (26.2×10^{-3} cm^{-1}) above the ground state. The character is $^3\pi-\pi^*$ as a result of an almost pure and HOMO → LUMO+1 transition. Although the computed energy is too high compared to the experimental value, this state can describe qualitatively the phosphorescence band centered at 468 nm (21.4×10^{-3} cm^{-1}) of **1** at 77 K.

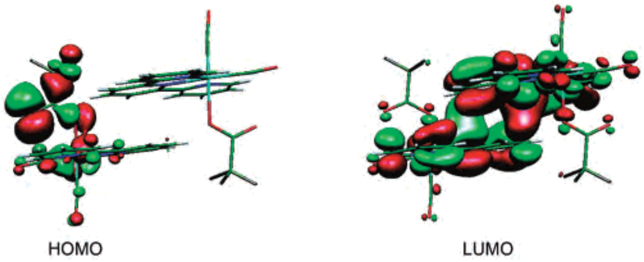

Figure 12. HOMO and LUMO orbitals for the triplet excited state of a [Ru(tpy)(CO)$_2$TFA]$^+$[PF$_6$]$^-$ dimer. The unpaired spins for the dimer in the triplet state are principally contained in these two orbitals.

The energy emission of [Ru(tpy)(CO)$_2$TFA]$^+$ has been evaluated as the vertical energy gap between the S$_0$ and T$_1$ energies, both evaluated at the optimized geometry of T$_1$. The value obtained is 14400 nm (693 cm^{-1} or 0.086 eV) suggesting how close the ground state and the lowest-lying triplet state are. Furthermore, among the eight triplet excited states computed starting from the lowest-lying triplet geometry, several have low energy. They range from 1436 to 620 nm (6.7×10^{-3} cm^{-1} to 16.1×10^{-3} cm^{-1} or 0.86−2.00 eV). The computation results seem to confirm the experimental results, where no triplet emission is observed at room temperature. These low-lying triplet states can provide deactivation pathways. However, the nature of the lowest-lying triplet state is closely related to the one observed for the free *cis*−*cis* tpy. The orbitals involved are tpy-centered, but in the case of the complex a significant orbital portion is present on the TFA group and on the metal-carbonyl moiety. In acetonitrile glass, the energy gap between this state and the ground state may increase, thus providing radiative decay. The band centered at 468 nm (21.4×10^{-3} cm^{-1}) could be rationalized by hypothesizing this mechanism.

Intermolecular Interactions and Spectral Assignment. For qualitative analysis of the concentration-dependent emission band at 603 nm we calculated the orbitals (Figure 12) and transition energies for a dimer of **1**. The transition between HOMO and LUMO can be used as an approximation of radiative triplet transitions.[62] Since this emission band has been observed both in the solid state and in solution, we chose to perform this calculation in vacuo (see Computational Details). Judging from the transition dipole moment, the HOMO and LUMO of the triplet state are more relevant to a radiative transition. The LUMO → HOMO transition involves a charge transfer. The energy difference is 1.94 eV, corresponding to a 632 nm emission. We performed an

---

(62) Dattelbaum, D. M.; Martin, R. L.; Schoonover, J. R.; Meyer, T. J. *J. Phys. Chem. A* **2004**, *108*, 3518−3526.

analysis to characterize the HOMO of the triplet state and found that 99% of the single electron density is on one of the two monomers, and 62% of it centers on the Ru atom, 12% centers on tpy, and 10% centers on TFA. The orbital plots of the dimer in the singlet are consistent with a description of this state as a result of metal-to-ligand charge-transfer excitation (where the two monomer units are practically independent). The weak absorption band observed at 470 nm in highly concentrated solution seems to confirm this assignment.

The proposed assignment is qualitative since no spectroscopic evidence for a particular dimer structure could be obtained in solution. Different geometries as well as oligomeric aggregates may be present both in the solid state and in solution. However, the proposed charge-transfer mechanism appears to be valid based on the computational studies and demonstrates how intermolecular weak interactions may play an important role changing indeed the electronic properties of molecules.

Conclusions

The importance of $\pi-\pi$ stacking to the photophysical properties of both the free ligand, tpy, and **1** at relatively high concentrations and low temperatures has been demonstrated. In the case of tpy, this is not surprising, but in the case of **1**, where the octahedral geometry precludes direct metal−metal interactions, the importance of these weak interactions is more surprising. That these same proposed interactions are seen in the solid-state structure of **1** suggests that where these are observed in the crystal lattice their importance to the solution properties of the complex should be investigated. Their persistence in solution and the use of TDDFT to understand their influence on photphysical properties could prove to be a valuable tool for extending the many applications of Ru(II)-polyimmine complexes.

Acknowledgment. J.B.A.R. and L.S. gratefully acknowledge support by NSF MCB-0517644 and by NIH COBRE RR-15583. E.R. acknowledges the support of the Department of Energy (DE-FG0201ER45869). We are indebted to Dr. F. Barigelletti (ISOF CNR, Bologna, Italy) for the helpful discussions. We acknowledge financial support of this work by Regione Piemonte.

Supporting Information Available: Crystallographic data in CIF format, electrochemistry, normal-mode analysis for $[Ru(tpy)(CO)_2TFA]^+[PF_6]^-$, and reaction of $K^+[Ru(CO)_3(TFA)_3]^-$ with 2,2′:6,2″-terpyridine. This material is available free of charge via the Internet at http://pubs.acs.org.

IC7010343